

ELECTRODYNAMICS OF SUPERCONDUCTORS EXPOSED TO HIGH FREQUENCY FIELDS

Ernst Helmut Brandt, Max-Planck-Institut für Metallforschung, Stuttgart, Germany*

Abstract

The electric losses in a bulk or film superconductor exposed to a parallel radio-frequency magnetic field may have three origins: In homogeneous vortex-free superconductors losses proportional to the frequency squared originate from the oscillating normal-conducting component of the charge carriers which is always present at temperatures $T > 0$. With increasing field amplitude the induced supercurrents approach the depairing current at which superconductivity breaks down. And finally, if magnetic vortices can penetrate the superconductor they typically cause large losses since they move driven by the AC supercurrent.

INTRODUCTION

The phenomenon of superconductivity was discovered in 1911 by Heike Kamerlingh-Onnes in Leiden. After he had achieved to liquify helium at the temperature of $T = 4.2\text{K}$ he observed that the resistivity of Hg became unmeasurably small below some “critical temperature” $T_c = 4.15\text{K}$. A sensitive method to measure the residual resistivity in this “superconducting state” is to observe the temporal decay of the persistent “supercurrents” in a ring, say of Pb ($T_c = 7.2\text{K}$), Sn ($T_c = 3.72\text{K}$), or Nb ($T_c = 7.2\text{K}$) by monitoring the magnetic field generated by the circulating current. It turned out [1] that the supercurrent does not decay measurably, even after several years. Ideally loss-free superconducting wires may thus be used to build coils which keep their magnetic field for years, after the windings have been loaded with current and then are cut short by a superconducting switch.

Thus, DC currents in a superconductor can flow practically loss-free if they are not too large. However, it turned out that alternating currents (AC) in superconductors are not completely loss-free, in particular at high frequencies (RF = radio frequencies, MW = microwave frequencies). There are essentially three effects which cause energy dissipation during current flow in superconductors:

(a) Even in ideally homogeneous bulk superconductors an electric field $E \propto \omega$ (with frequency $\omega/2\pi$) is required to accelerate the “superconducting electrons”, the Cooper pairs of the microscopic BCS theory [2]. This electric field also moves the “normalconducting” electrons that are always present at finite temperatures $T > 0$. The dissipated power of this effect is $\propto E^2 \propto \omega^2$.

(b) When the current density inside the superconductor reaches the depairing current density j_{dp} , the superconducting order parameter is suppressed to zero at the place

where $j = j_{dp}$. This means superconductivity disappears and electric losses appear. This nucleation of the normal state typically occurs at the specimen surface or in the center of Abrikosov vortices. In particular, when an increasing magnetic field H_a is applied along a superconducting half space $x > 0$ one initially has $j(x) = (H_a/\lambda) \exp(-x/\lambda)$ when $j \ll j_{dp}$, but when H_a reaches the thermodynamic critical field $H_c = \Phi_0/(\sqrt{8}\pi\lambda\xi\mu_0)$ one has $j \approx j_{dp}$ near the surface, thus one has $j_{dp} \approx H_c/\lambda$. Here $\Phi_0 = h/2e = 2.07 \cdot 10^{-15}\text{ Tm}^2$ is the quantum of magnetic flux, λ is the magnetic penetration depth, and ξ is the superconducting coherence length. Within Ginzburg-Landau (GL) theory, valid near $T = T_c$, the lengths $\lambda(T) = \kappa\xi(T) \propto (T_c - T)^{-1/2}$ diverge as $T \rightarrow T_c$, but the GL parameter $\kappa = \lambda/\xi$ is independent of temperature T .

(c) Large dissipation may be caused by vortices inside the superconductor. These move under the action of the induced AC current, which exerts a Lorentz force on the vortices and causes them to oscillate and dissipate energy. At high frequencies the amplitude of this oscillation is smaller than the range of possible pinning forces caused by material inhomogeneities, e.g., precipitates or defects in the crystal lattice. This vortex dissipation then cannot be suppressed by introducing pins.

For a flat bulk type-II superconductor (defined by $\kappa > 1/\sqrt{2}$) in thermodynamic equilibrium it is favorable that part of the magnetic flux penetrates in form of Abrikosov vortices when the applied field H_a equals or exceeds the lower critical field $H_{c1} \approx (\Phi_0/4\pi\lambda^2\mu_0)(\ln\kappa + 0.5)$ (for $\kappa > 1.5$) and has not yet reached the upper critical field $H_{c2} \approx \Phi_0/(2\pi\xi^2\mu_0)$ where superconductivity vanishes. The penetration of vortices at an ideally flat surface may be delayed by a surface barrier leading to a higher penetration field $H_p \approx H_c \geq H_{c1}$ (overheating). On the other hand, with superconductors of finite size, demagnetization effects may allow the vortices to penetrate already at much lower fields. In particular, for a large film of width w and thickness $d \ll w$, the penetration field is strongly reduced, $H_p/H_{c1} \approx d/w \dots \sqrt{d/w} \ll 1$ depending on the edge profile, see below. An infinitely large thin film will thus be penetrated by any perpendicular magnetic field component, even if very small.

AC RESPONSE OF VORTEX-FREE SUPERCONDUCTORS

The puzzling fact that superconductors may carry loss-free DC current but AC currents exhibit electric losses, was explained by the two-fluid model of Gorter and Casimir in 1934 [1]. Later, the microscopic BCS Theory [2] essen-

* ehb @ mf.mpg.de

tially confirmed the two-fluid picture, giving for its phenomenological parameters a microscopic interpretation and explicit expressions.

Two-Fluid Model

The phenomenological two-fluid model assumes that the total electron density is composed of the density of superconducting electrons n_s and that of normal electrons n_n , which have different relaxation times τ_s and τ_n . Historically, Gorter and Casimir assumed $n_n \propto t^4$ ($t = T/T_c$) and $n_s \propto 1 - t^4$. As in the Drude model [1], the drift velocity \mathbf{v} of each of these two fluids should obey a Newton law,

$$m d\mathbf{v}/dt = e\mathbf{E} - m\mathbf{v}/\tau \quad (1)$$

with m and e the mass and charge of the electron. The total current density $\mathbf{J} = \mathbf{J}_s + \mathbf{J}_n$ is the sum of the supercurrent $\mathbf{J}_s = en_s\mathbf{v}_s$ and the normal current $\mathbf{J}_n = en_n\mathbf{v}_n$. (In all other Sections of this paper the current density is denoted by \mathbf{j} .) If one assumes $\tau_s = \infty$ one obtains from Eq. (1) the first London equation

$$d\mathbf{J}_s/dt = (n_se^2/m)\mathbf{E} = \mathbf{E}/(\mu_0\lambda^2) \quad (2)$$

with $\lambda = (m/n_se^2\mu_0)^{1/2}$ the London depth. In the London gauge where $\mathbf{E} = -d\mathbf{A}/dt$ (induction law) Eq. (2) may be written in form of the second London equation $\mathbf{J}_s = (\mu_0\lambda^2)^{-1}\mathbf{A}$. For the normal electrons one may assume $\tau_n \ll 1/\omega$ with periodic electric field $E \propto \exp(i\omega t)$. This gives for the normal current

$$\mathbf{J}_n = (n_ne^2\tau_n/m)\mathbf{E}. \quad (3)$$

Defining the complex conductivity $\sigma(\omega) = \sigma_1(\omega) - i\sigma_2(\omega)$ by $\mathbf{J} = \sigma(\omega)\mathbf{E} \propto \exp(i\omega t)$, one obtains

$$\begin{aligned} \sigma_1(\omega) &= (\pi n_se^2/m\omega) \delta(\omega) + n_ne^2\tau_n/m, \\ \sigma_2(\omega) &= n_se^2/m\omega = (\mu_0\lambda^2\omega)^{-1} \gg \sigma_1. \end{aligned} \quad (4)$$

For a normal conductor this yields $\sigma_1 = \sigma_n$, $\sigma_2 = 0$, and the skin depth $\delta_{\text{skin}} = (2/\mu_0\sigma_n\omega)^{1/2}$. For superconductors at $\omega = 0$ the δ -function in σ_1 reflects the ideal DC conductivity, while at finite frequencies the inductive part dominates, $\sigma_2 \gg \sigma_1$. However, the small dissipative part $\sigma_1 = n_ne^2\tau_n/m$ is important since it causes the AC losses. In the situation with an AC magnetic field parallel to the superconductor surface, the current is forced (a current bias as opposed to a voltage bias) and one has a dissipation per unit volume $\rho J^2 = \text{Re}\{1/\sigma\}J^2 \approx (\sigma_1/\sigma_2^2)J^2 \approx \sigma_1 E^2$ since $\sigma_1 \ll \sigma_2$. The dissipation is thus proportional to $n_n\omega^2$.

The sum $\sigma = \sigma_1 - i\sigma_2$ is analogous to a circuit of a resistive channel $1/R \propto \sigma_1$ in parallel to an inductive channel of admittance $1/i\omega L \propto \sigma_2$. Below a frequency $\omega_0 = R/L$ this circuit is mainly inductive and above mainly resistive. The ratio of the currents in the two channels is $J_s/J_n = n_s/(n_n\omega\tau)$. This defines a crossover frequency $\omega \approx (n_s/n_n)(1/\tau_n) \approx (n_s/n_n) \cdot 10^{11} \text{ Hz}$ [1].

When the superconductor forms the inner wall of a microwave cavity with incident parallel magnetic field of amplitude H_{inc} , this wave is almost ideally reflected by the wall since a surface screening current $J_s = 2H_{\text{inc}}$ is induced. The small dissipated power per unit area is then $P_s = J_s^2 R_s$, where

$$R_s = \delta^{-1} \text{Re}\{1/\sigma\} = \delta^{-1} \sigma_1/|\sigma|^2 \approx \delta^{-1} \sigma_1/\sigma_2^2 \quad (5)$$

is the surface resistance (e.g. in units Ω). Here $\delta = [2/\mu_0(|\sigma| + \sigma_2)\omega]^{1/2}$ is the general skin depth reducing to the superconducting penetration depth λ or to the skin depth δ_{skin} in the super or normal conducting limits. For the superconducting wall one has $R_s \approx \sigma_1\mu_0^2\lambda^3\omega^2/2$ and the absorbed versus incident power of this wall is [1]

$$\frac{P_{\text{abs}}}{P_{\text{inc}}} = \frac{J_s^2 R_s}{c\mu_0 H_{\text{inc}}^2} = \frac{4R_s}{c\mu_0} \approx \frac{1}{Q}. \quad (6)$$

The quality factor Q of the superconducting cavity is thus inversely proportional to $R_s \propto Q^{-1} \propto n_n\omega^2$.

Microscopic Theory

After the BCS theory [2] had given the microscopic explanation of superconductivity, the complex AC conductivity was calculated within this weak-coupling theory [3, 4]. In the extreme local limit ($\lambda \ll \xi_0 = \hbar v_F/\pi\Delta$ with v_F = Fermi velocity and Δ = energy gap; this assumption actually is not satisfied for type-II superconductors with GL parameter $\kappa > 0.7$), in the impure limit (electron mean free path $l = v_F\tau \ll \xi_0$), and for frequencies below the energy-gap frequency ($\hbar\nu < 2\Delta$, $\nu = \omega/2\pi$) the resulting AC conductivity may be expressed as two integrals over an energy variable,

$$\frac{\sigma_{1,2}}{\sigma_n} = \int f_{1,2}(\epsilon, \Delta, T, \omega) d\epsilon, \quad (7)$$

where $\sigma_n = ne^2\tau/m = ne^2l/p_F$ ($p_F = mv_F$ = Fermi momentum, n = electron density) is the Drude conductivity in the normal state and f_1 and f_2 are some functions. Evaluating these integrals for the case $\omega \ll T \ll \Delta$ (in units $\hbar = k_B = 1$) one obtains [5]

$$\begin{aligned} \frac{\sigma_1}{\sigma_n} &= \frac{2\Delta}{T} \exp\left(-\frac{\Delta}{T}\right) \ln \frac{9T}{4\omega}, \\ \frac{\sigma_2}{\sigma_n} &= \frac{\pi\Delta}{\omega}. \end{aligned} \quad (8)$$

The dissipative part σ_1 and inductive part σ_2 may be written in the form of the two-fluid model:

$$\begin{aligned} \sigma_1 &\approx n_{qp} e^2 l / p_F, \\ \sigma_2 &\approx n_s e^2 / m\omega, \end{aligned} \quad (9)$$

where n_{qp} is the quasiparticle density (replacing the normal electron density n_n of the two-fluid model) and n_s the superconducting electron density,

$$\begin{aligned} n_{qp} &= n \frac{\Delta}{T} \exp\left(-\frac{\Delta}{T}\right) 2 \ln \frac{9T}{4\omega}, \\ n_s &= n l / \xi_0. \end{aligned} \quad (10)$$

The quality factor Q of the resonator is now

$$Q^{-1} \propto R_s \approx \frac{1}{2} \mu_0^2 \lambda^3 \sigma_1 \omega^2 \propto n_{qp} \omega^2. \quad (11)$$

Since the quasiparticle density $n_{qp} \sim \exp(-\Delta/T)$ strongly decreases at low temperatures T , Q should increase drastically. Note that with increasing purity (increasing l) σ_1 increases but the penetration depth $\lambda \approx \lambda_{\text{pure}} \sqrt{1 + \xi_0/l}$ decreases in Eq. (11). Thus, maximum Q is reached at some intermediate, not too high purity of the superconductor.

High-Purity Niobium

For the high-purity Nb used in the TESLA cavities, the frequency dependent surface resistance has been computed by Kurt Scharnberg within the Eliashberg model that extends the BCS model to strong coupling superconductors [6]. Strong (electron-phonon) coupling effects change the amplitude and the temperature dependence of the gap parameter, they lead to a renormalization (enhancement) of the quasiparticle mass, which in turn affects the London penetration depth, and they result in temperature and energy dependent quasiparticle lifetimes. The electron-phonon interaction enters in form of the Eliashberg function $\alpha^2 F(\omega)$ which was taken from tunneling experiments. A Coulomb pseudopotential $\mu^* = 0.17$ and a Coulomb cut-off $\omega_c = 240$ meV were used. At sufficiently low T and low ω of the incident radiation, inelastic scattering is negligible and only disorder induced elastic scattering is important, which is parameterized by the normal state scattering rate $\Gamma_N = 1/2\tau$. This is fit to the surface resistance R_s measured at $\nu = 1.3$ GHz, yielding $\Gamma_N \approx 1$ meV and $\tau \approx 3 \cdot 10^{-13}$ sec. Nonlocal effects (wave vector $q > 0$) were disregarded, which is partly corrected for by using the lifetime τ fitted at 1.3 GHz.

With these assumptions the surface resistance $R_s \approx \frac{1}{2} \sigma_1 \mu_0^2 \lambda^3 \omega^2$ of high-purity Nb was computed at $T = 2$ K. Note that R_s is related to the reflectivity r of the metal by $R_s = (Z_0/4)(1 - r)$ where $Z_0 = (\epsilon_0 c)^{-1} = 377 \Omega$ is the impedance of the vacuum. Starting from $R_s \approx 20$ n Ω at 1.3 GHz the resistance rises to a few $\mu\Omega$ at 600 GHz and then exhibits a large step at 750 GHz to a value of 15 m Ω . Above this energy-gap frequency $\nu = 2\Delta/h$ one has nearly constant R_s till at least 2000 GHz.

VORTICES IN SUPERCONDUCTORS

Ginzburg-Landau and London Theories

Before the microscopic explanation of superconductivity was given in 1957 by BCS [2] there were very powerful phenomenological theories that were able to describe the thermodynamic and electrodynamic behavior of superconductors. In 1935 Fritz and Heinz London established the London theory, see Eq.(2) above, and in 1952 Vitalii Ginzburg and Lev Landau conceived the Ginzburg-Landau (GL) theory. The GL theory may be written as a variational

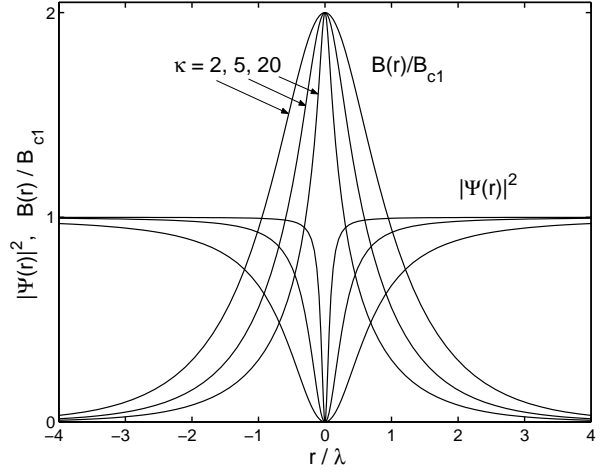


Figure 1: Magnetic field $B(r)$ and order parameter $|\psi(r)|^2$ of an isolated flux line calculated from Ginzburg-Landau theory for GL parameters $\kappa = 2, 5$, and 20 . Note that the field in the vortex center is $B(0) \approx 2B_{c1}$.

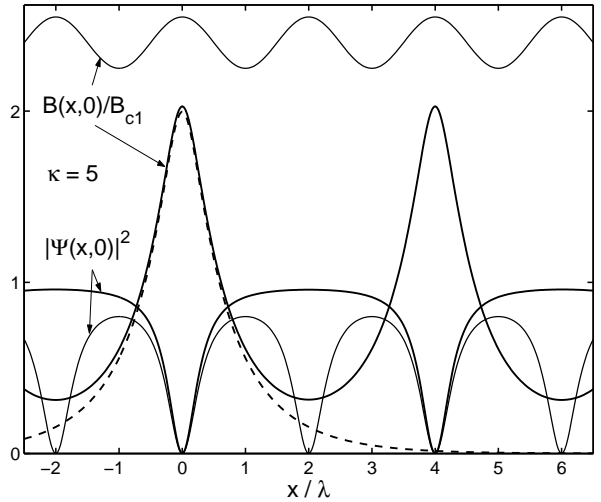


Figure 2: Two profiles of the magnetic field $B(x, y)$ and order parameter $|\Psi(x, y)|^2$ taken along the x axis (a nearest neighbor direction) for vortex lattices with lattice spacings $a = 4\lambda$ (bold lines) and $a = 2\lambda$ (thin lines). The dashed line shows the magnetic field of an isolated flux line from Fig. 1. Calculated from GL theory for $\kappa = 5$ [10].

problem that minimizes the spatially averaged GL free energy density,

$$\langle -|\psi|^2 + \frac{1}{2}|\psi|^4 + |(i\xi\nabla + \mathbf{A})\psi|^2 + (\lambda\nabla \times \mathbf{A})^2 \rangle = \text{Minimum}. \quad (12)$$

Here $\psi(\mathbf{r})$ is the complex GL-function, or order parameter, and $\mathbf{A}(\mathbf{r})$ the vector potential of the magnetic induction $\mathbf{B} = \nabla \times \mathbf{A}$. The two lengths are the magnetic penetration depth λ (usually taken as unit length) and the GL coherence length ξ ; both lengths diverge as the temperature T approaches the critical temperature T_c ,

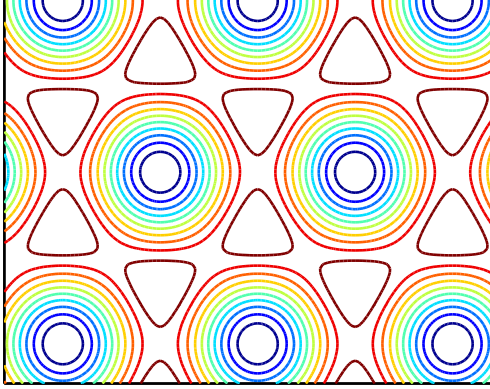


Figure 3: Current stream lines, coinciding with the contours of $B(x, y)$ and $|\psi(x, y)|^2$. Abrikosov solution for the ideal vortex lattice near the upper critical field B_{c2} .

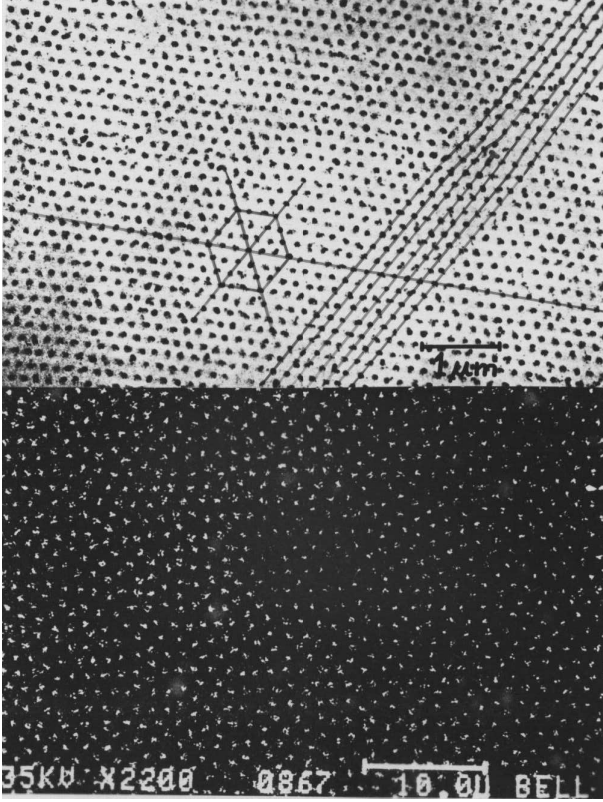


Figure 4: Vortex lattice made visible by decoration with iron micro-crystallites. Top: Nb disk, 1 mm thick, 4 mm diameter, $T = 4$ K, $B_a = 985$ Gauss, vortex spacing $a = 170$ nm (U. Essmann and H. Träuble 1968). Bottom: $\text{YBa}_2\text{Cu}_3\text{O}_{7-\delta}$, $T = 77$ K, $B_a = 20$ Gauss, $a = 1200$ nm (D. Bishop and P. Gammel 1987).

$\lambda \propto \xi \propto (T_c - T)^{-1/2}$. Their ratio, the GL parameter $\kappa = \lambda/\xi$ within GL theory (valid near T_c) is independent of T .

The GL theory can be derived from the microscopic BCS theory (L. P. Gor'kov 1959) in the limit $T_c - T \ll T_c$, yielding for the GL function $\psi(\mathbf{r}) = \Delta(\mathbf{r})/\Delta_{\text{BCS}}$ where

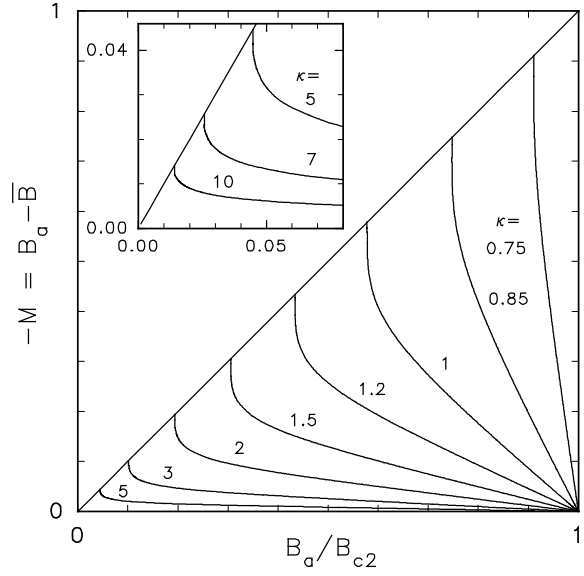


Figure 5: Ideal reversible magnetization curves of a long superconducting cylinder or slab in parallel field B_a computed from GL theory [10].

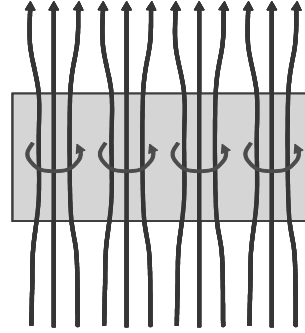


Figure 6: Magnetic field lines of vortex lines in and near a superconductor of finite size, and the circulating super currents (schematic).

Δ is the energy gap function. The London theory follows from GL theory in the cases when the magnitude of the order parameter is nearly constant, $|\psi| \approx 1$. This condition is fulfilled when ξ is small as compared to the specimen extension and to λ , requiring $\kappa \gg 1$. An arrangement of straight or arbitrarily curved vortex lines positioned at $\mathbf{r}_\nu(z) = [x_\nu(z), y_\nu(z), z]$ ($\nu = 1, 2, 3 \dots$) then has a magnetic field that obeys the London equation modified by adding δ functions centered at the vortex cores,

$$(1 - \lambda^2 \nabla^2) \mathbf{B}(\mathbf{r}) = \Phi_0 \sum_{\nu} \int d\mathbf{r}_{\nu} \delta_3(\mathbf{r} - \mathbf{r}_{\nu}). \quad (13)$$

Ideal Vortex Lattice

In 1957 Alexei Abrikosov, a thesis student of Lev Landau in Moscow, obtained a periodic solution of the Ginzburg-Landau equations and recognized that this corresponds to a lattice of vortices of supercurrent, circulat-

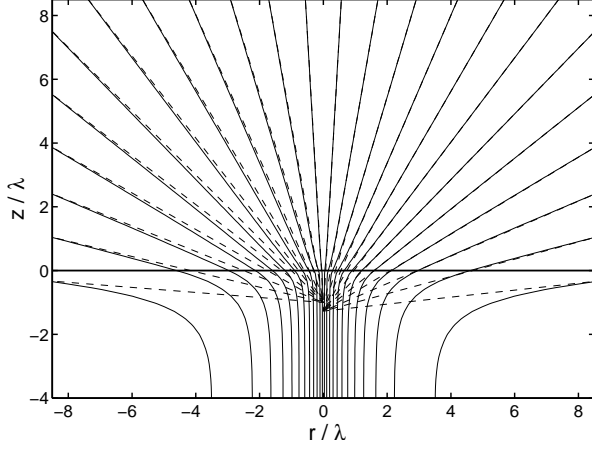


Figure 7: Magnetic field lines of a single vortex in a superconducting film of thickness $d = 8\lambda$ (or half space $z \leq 0$). Analytical solution of London theory [11].

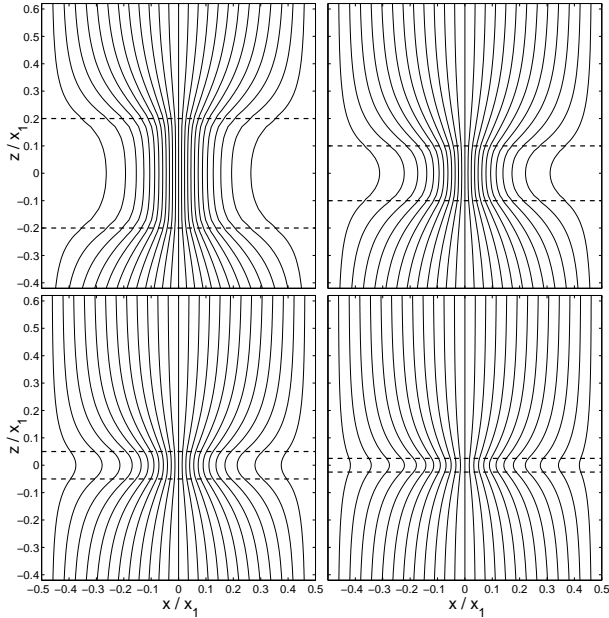


Figure 8: Magnetic field lines of the periodic vortex lattice in films of thicknesses $d = 4\lambda, 2\lambda, \lambda$, and $\lambda/2$. From GL theory for $\kappa = 1.4$ and $\bar{B}/B_{c2} = 0.04$ [12]. The dashed lines mark the film surfaces. x_1 = vortex spacing.

ing around each zero of the order parameter and carrying a quantum of magnetic flux Φ_0 ; these vortex lines (or flux lines, fluxons) are energetically favorable when the applied magnetic field is between a lower and a higher critical field, $H_{c1} \leq H_{c2}$ (see Introduction and below). This solution exists in bulk superconductors with GL parameter $\kappa \geq 1/\sqrt{2}$, called type-II superconductors. For this theoretical discovery Abrikosov received the Nobel Prize in Physics in 2003.

Figure 1 shows the magnetic field $B(r)$ and the order parameter $|\psi(r)|^2$ of one isolated vortex line for three values of the GL parameter $\kappa = 2, 5, 20$. One can see that B decays over the length λ and the vortex core has a radius $\approx \xi$.

For such not too small values of κ to a good approximation the vortex field is the London solution, with the central singularity smoothened over the core radius $r_c \approx \sqrt{2}\xi$ [7, 8],

$$B_v(r) \approx \frac{\Phi_0}{2\pi\lambda^2} K_0\left(\frac{\sqrt{r^2 + r_c^2}}{\lambda}\right)$$

$$K_0(x) = \begin{cases} \ln(1.123/x), & x \ll 1 \\ \sqrt{\pi/2x} \exp(-x), & x \gg 1 \end{cases} \quad (14)$$

$K_0(x)$ is a modified Bessel function. The interaction energy of two vortices at a distance $x \gg \xi$ is $U_{\text{int}} = \Phi_0 B_v(x)/\mu_0$.

Figure 2 shows cross sections of $B(x, y)$ and $|\psi(x, y)|^2$ along the nearest neighbor direction $y = 0$ of the ideal triangular vortex lattice for two values of the average induction $\bar{B} = \langle B \rangle$ (with vortex spacing $a = 2\lambda$ and $a = 4\lambda$) and $\kappa = 5$. The dashed line is $B(r)$ for the isolated vortex. Figure 3 shows the contour lines of $B(x, y)$ near B_{c2} for the triangular vortex lattice. These lines coincide with the contours of $|\psi(x, y)|^2$ and with the stream lines of the supercurrents.

The vortex lattice was first observed in the electron microscope by U. Essman and H. Träuble [9] at our Max Planck Institute in Stuttgart, by decoration of the surface of a Nb disk with “magnetic smoke” generated by evaporating an iron wire in a He atmosphere of 1 Torr, see Fig. 4. The magnetization $-M = B_a - \bar{B}$ of the superconductor calculated numerically [10] as function of the applied magnetic field B_a is depicted in Fig. 5 for ideal (pin-free) long superconductor cylinders or slabs in parallel B_a (i.e., in absence of demagnetization effects) with various $\kappa = 0.707 \dots 10$. At $\kappa = 1/\sqrt{2}$ one has $B_{c1} = B_c = B_{c2}$ and the curve $M(B_a)$ is the same as for type-I superconductors (with $\kappa < 1/\sqrt{2}$), namely, $\bar{B} = 0$, $-M = B_a$ (no penetrated flux) for $B_a < B_{c2}$ and $\bar{B} = B_a$, $M = 0$ (complete penetration of flux) for $B_a > B_{c2}$.

When the superconductor is not a long cylinder or slab in parallel field, demagnetization effects shear the magnetization curves of Fig. 5 and reduce the field of first vortex penetration, see below. The vortices end at the upper and lower surface of finite-size specimens and send their magnetic field lines into the surrounding vacuum, see Fig. 6. The resulting modulation of $B(x, y)$ just outside the surface can be observed by decoration (Fig. 4) and by magneto-optics or Hall probes. The magnetic field lines of one vortex in a thick film in a perpendicular magnetic field are depicted in Fig. 7 as obtained from London theory in [11]. Figure 8 shows the field lines of the periodic vortex lattice in films of thicknesses $d = 4\lambda, 2\lambda, \lambda$, and $\lambda/2$ as calculated in [12].

Losses by Moving Vortices

When a supercurrent flows in a superconductor, either applied by contacts or caused by a gradient or curvature of the local magnetic field, this current density \mathbf{j} exerts a Lorentz force $\mathbf{f} = \mathbf{j} \times \hat{\mathbf{z}}\Phi_0$ on a vortex. The Lorentz force density on a vortex lattice is $\mathbf{F} = \mathbf{j} \times \bar{\mathbf{B}}$. Neglecting a small Hall effect, the vortices move along this force with velocity

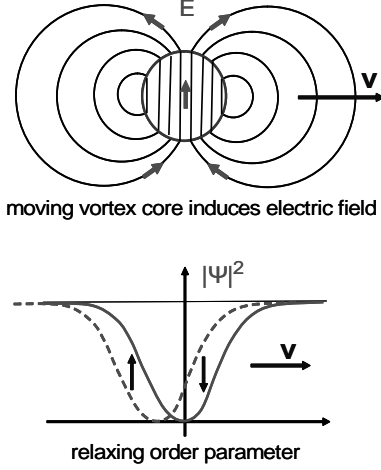


Figure 9: Visualization of the origin of energy dissipation when a vortex moves with velocity v . Top: the dipolar electric field lines induced by this motion run also through the normal conducting core (Bardeen-Stephen model). Bottom: During motion of the vortex core the order parameter relaxes (Tinkham term).

$\mathbf{v} = \eta^{-1} \mathbf{F}$ where η is a drag coefficient or viscosity. The vortex motion induces an average electric field

$$\mathbf{E} = \bar{\mathbf{B}} \times \mathbf{v} = \eta^{-1} \bar{\mathbf{B}} \times (\mathbf{j} \times \bar{\mathbf{B}}) = \rho_{\text{ff}} \mathbf{j}, \quad (15)$$

$$\rho_{\text{ff}} \approx (\bar{B}/B_{c2}) \rho_n. \quad (16)$$

Here ρ_{ff} is the flux-flow velocity, which at large average inductions \bar{B} is comparable to the normal resistivity of the superconductor at that temperature (measurable by applying a large field $B_a > B_{c2}$). However, when only a few vortices have penetrated ($\bar{B} \ll B_{c2}$) one has much smaller resistivity $\rho_{\text{ff}} \ll \rho_n$. But even then the vortex-caused dissipation at low T is typically much larger than the dissipation caused by the normal excitations.

Where does this resistive dissipation come from? There are two effects of comparable size, see Fig. 9. First, as pointed out by Bardeen and Stephen [1, 13], the motion of the magnetic field induces a dipolar electric field that drives current through the superconductor and through the vortex core. If the vortex core is modelled as a normal conducting tube of radius $r_c \approx \xi$, the normal currents inside the vortex core dissipate energy that leads to the ρ_{ff} of Eq. (16). Second, as stated by Tinkham [1, 14], the moving vortex core means that at a given position the order parameter $|\psi|^2$ goes down and up again when the core passes. If one assumes a delay of the recovery of $|\psi|^2$ by a relaxation time $\tau \approx \hbar/\Delta$ one obtains an additional dissipation of the order of Eq. (16). These two sources of losses are nice for physical understanding. In the exact calculation of the dissipation of a moving vortex lattice from time-dependent GL theory [15] these two sources cannot be separated but the approximate Eq. (16) is essentially confirmed [16], also by microscopic theory [17]. The numerical and also the measured flux-flow resistivity in the middle between the exact

values 0 and ρ_n is somewhat smaller than the Eq. (16), i.e., for constant current source the real dissipation is lower.

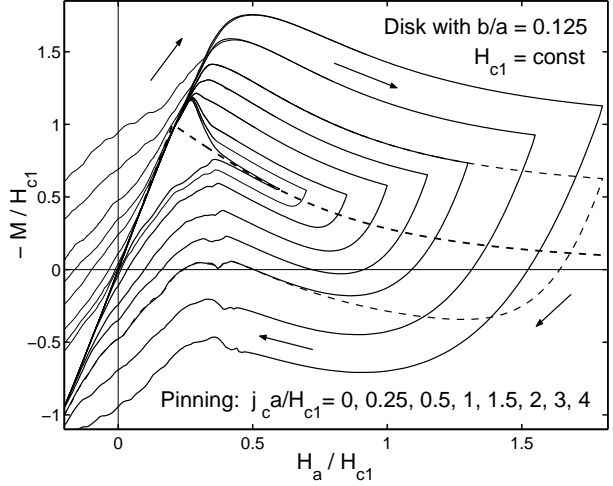


Figure 10: Irreversible magnetization curves $M(H_a)$ for a disk with radius a and thickness $2b$, $b/a = 0.125$, for various pinning strengths measured by the parameter aj_c/H_{c1} . The large hysteresis loop belongs to strong pinning $aj_c/H_{c1} = 4$. The small central loop is for the pin-free disk, whose vortex distribution is shown in Fig. 11. The reversible magnetization curve of a pin-free ellipsoid with same initial slope as $M(H_a)$ is shown as dashed line.

Pinning of Vortices

When the material is inhomogeneous on the microscopic length scale of the vortex core ξ , then the vortices are pinned and cannot move as long as the Lorentz force does not exceed the pinning force, or the current density j is smaller than the critical current density j_c , see the reviews [18, 19, 20]. In this way the electric losses caused by flux flow can be avoided, and completely loss-free conductors of DC current can be tailored by introducing appropriate pinning centers into the material, e.g., precipitates and crystal lattice defects. For AC currents small losses remain, however. One source of AC dissipation is due to the (albeit small) concentration of normal carriers or excitations and can be understood from the two-fluid model as discussed above. The other source is the oscillation of vortices in the pinning wells. At small displacements u from their equilibrium position one may assume linear elastic binding of the vortices to the pins, with a force density $-ku$. Adding to this the viscose drag force $-\eta\dot{u}$ and the Lorentz force one obtains the force balance equation in an AC current $\mathbf{j}_{ac} \propto \exp(i\omega t)$,

$$\mathbf{j}_{ac} \times \bar{\mathbf{B}} = -k\mathbf{u} - i\omega\eta\mathbf{u}. \quad (17)$$

One can see that at frequencies above k/η , of order $\omega/2\pi > 10^7$ Hz, the viscose force dominates [21]. Pinning thus cannot prevent vortex oscillations at high fre-

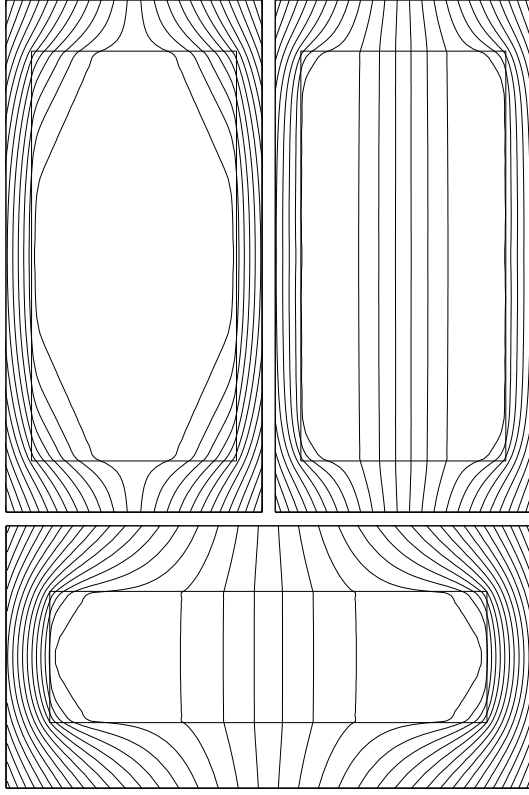


Figure 11: Penetration of vortex lines into pin-free cylinders with radius a and height $2b$. Top: $b/a = 2$. Bottom: $b/a = 0.3$. Forced by the applied field H_a , the vortices enter from the corners, but only when the applied field has reached some threshold field do they jump to the middle leaving a vortex-free zone near the surface. With further increasing H_a the vortices eventually fill the cylinder uniformly from the middle. This delayed penetration without pinning is called geometrical barrier. Such a barrier is absent only for ellipsoid-shaped specimens.

quencies. This vortex-caused dissipation increases as ω^2 , like the quasiparticle dissipation, cf. Eq. (11).

Interesting theoretical problems are the statistical summation of random pinning forces to obtain the critical current density j_c , and the problem of thermally activated depinning [18, 19, 20]. The latter leads to vortex motion even at small currents densities $j < j_c$ due to finite temperature. This flux creep may be described by a highly nonlinear resistivity. In particular, a logarithmic dispersive activation energy for depinning, $U(j) = U_0 \ln(j_c/j)$, leads to an often observed power-law current-voltage curve,

$$E(j) = E_0 \exp[-U(j)/k_B T] = E_0 (j/j_c)^n \quad (18)$$

with a creep exponent $n = U_0/k_B T$. For $n = 1$ one has Ohmic behavior [free flux flow, Eq. (15)], for $n \gg 1$ one has flux creep, and in the limit $n \rightarrow \infty$ this power law yields the Bean model, in which j is either 0 or j_c : When at some position one has $j > j_c$, the vortices rearrange immediately such that j is reduced to j_c again. This concept

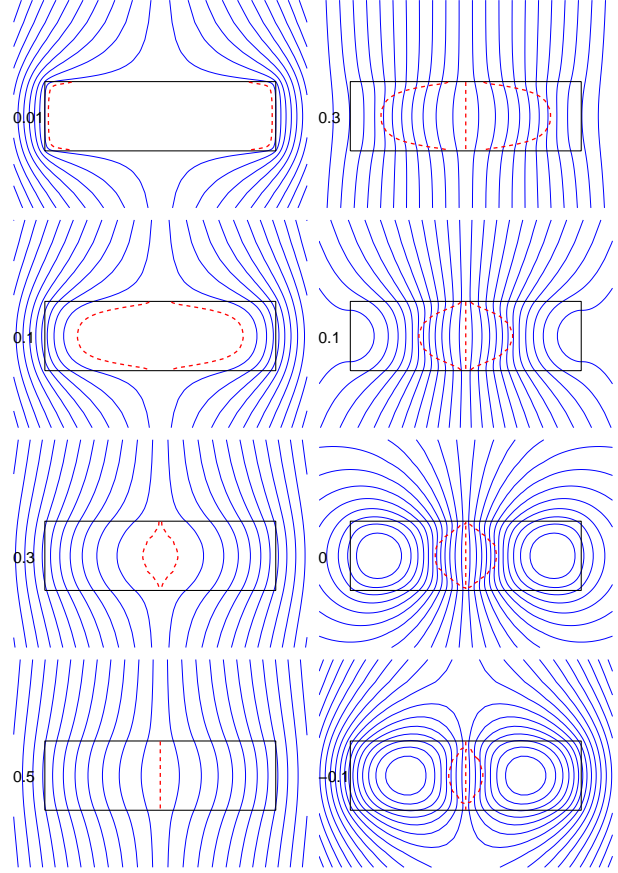


Figure 12: Bean model with constant critical current density j_c for a superconducting bar with rectangular cross section $2a \times 2b$ ($b/a = 0.35$) put into a perpendicular magnetic field H_a that first increases from 0 to 0.5 (left column) and then decreases again (right column). The parameter 0.01, 0.1, 0.3, 0.5, 0.3, 0.1, 0, -0.1 is $H_a/(a j_c)$. Shown are the magnetic field lines (solid lines) and the penetrating fronts (dashed lines) where the current density j (flowing along the bar) jumps from $\pm j_c$ to 0 (in the field-free and current-free core) or from j_c to $-j_c$ (after full penetration of flux).

is useful for DC currents and at not too high frequencies where the pinning forces exceed the viscous drag force.

Geometry Effects

The electromagnetic properties of a superconductor (and of any conductor or isolator) depend not only on the material but also on the geometry of the problem, i.e., on the shape of the specimen and on the way a magnetic or electric field is applied. For example, the reversible magnetization curves of a pin-free superconductor in Fig. 5 apply to the unrealistic case of very long slabs or cylinders in exactly parallel field, where demagnetization effects are absent. For the still unrealistic situation of a perfect ellipsoidal shape one may calculate from these ideal curves the reversible magnetization curves of any ellipsoid by using the concept of the demagnetization factor. But when

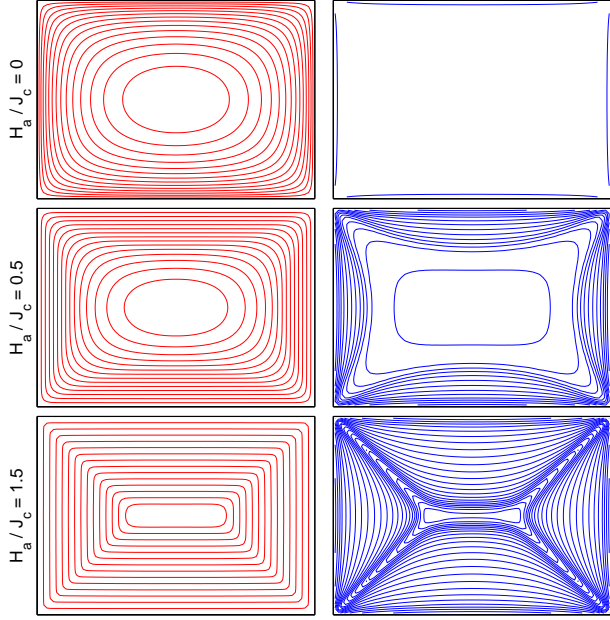


Figure 13: Bean model for the penetration of a perpendicular magnetic field $B_a = \mu_0 H_a$ into a thin rectangular film with thickness $d \ll$ width. The parameter $H_a/J_c = 0, 0.5, 1.5$ measures H_a in units of the critical sheet current $J_c = dj_c$. Shown are the stream lines of the sheet current in the film, $\mathbf{J}(x, y) = \int \mathbf{j}(x, y, z) dz$ (left), and the contour lines of the magnetic field $B_z(x, y)$ in the plane $z = 0$ of the film (right).

the specimen shape is not an ellipsoid, then even for a pin-free superconductor the magnetization curves have to be computed numerically, since now the induction (or vortex density) inside the specimen is no longer spatially constant.

It turns out that even without pinning such magnetization curves in general show a hysteresis, i.e., they are irreversible and depend on the magnetic history, see Fig. 10. This irreversibility is due to a geometric barrier [22, 23] for the penetration of vortices as illustrated in Fig. 11 for cylinders (or long bars) with rectangular cross section: When the applied uniform field H_a is increased, vortex lines enter at the corners, pulled by the screening currents (Meissner currents) that flow at the surface, and held back by their line tension (like a rubber band). With increasing H_a the vortices penetrate deeper and become longer. When the vortices from two corners meet at the equator, they connect and form one long vortex line that contracts and immediately jumps to the specimen center. During this rapid jump all their elastic energy is dissipated by the viscose drag force $F = \eta v$, see text above Eq. (15). With further increasing H_a more vortices jump to the center, crossing the flux-free zone near the surface, and eventually the entire specimen is filled with vortices coming from the growing central zone.

Flux penetration thus occurs with a threshold, over a “geometrical barrier”. The sudden onset of flux penetration to the center leads to the sharp maximum in the small (inner,

pin-free) hysteresis loop of $M(H_a)$ in Fig. 10. When H_a is decreased again, the vortices leave the specimen essentially without barrier, and at $H_a = 0$ all vortices have left, i.e., one has $\bar{B} = 0$ and also $M = 0$ (since no screening currents flow anymore). The perpendicular field at which the first vortices enter at the corners of a pin-free long strip and a circular disk, both with rectangular cross section $2a \times 2b$, was computed in [23]:

$$\begin{aligned} H_{\text{pen}}^{\text{strip}} &\approx H_{c1} \tanh \sqrt{0.36 b/a}, \\ H_{\text{pen}}^{\text{disk}} &\approx H_{c1} \tanh \sqrt{0.67 b/a}. \end{aligned} \quad (19)$$

In the presence of pinning the hysteresis loops of $M(H_a)$ in Fig. 10 become larger. The area of such loops is the energy dissipated during one cycle due to depinning of vortices. When H_{c1} is negligibly small as compared to H_a , the hysteresis curves and the vortex density and currents in a superconductor with pinning may be computed by treating it as a nonlinear conductor, Eq. (18). Figure 12 shows how the magnetic field lines (and vortices) penetrate and exit a thick disk with pinning when an axial H_a is first increased beyond the field of full penetration, and then is decreased again [24, 25]. The chosen large creep exponent $n = 50$ practically reproduces the Bean model.

Figures 10, 11, and 12 were computed by time-integration of an equation for the (scalar) current density j inside the superconductor; this method implicitly accounts for the infinitely extended magnetic stray field outside the specimen, without need to compute it and to cut it off. From the resulting current density the magnetic field lines are then easily calculated by the Biot-Savart law.

A completely different geometry is shown in Fig. 13, namely, the current stream lines and the contours of the magnetic field $B_z(x, y)$ in a thin film or platelet of rectangular shape [26] with pinning and large creep exponent $n = 50$ corresponding to the Bean model like in Fig. 12. An increasing magnetic field H_a is applied perpendicular to the film. Initially, when $H_a \ll J_c = dj_c$ is small, no magnetic flux penetrates the film, i.e., the circulating screening currents generate a magnetic field that in the film area is constant (of size $-H_a$) and exactly compensates the applied field H_a . With increasing H_a , magnetic flux penetrates mainly from the middle of the sides of the rectangle (not from the corners), leaving still a flux-free zone in the middle. At and beyond some field of full penetration the current stream lines are concentric rectangles of constant distance, since the magnitude of the sheet current has saturated to the constant value $J_c = dj_c$. The magnetic field has then penetrated to the center, and the contour lines of $B_z(x, y)$ do not change anymore with further increasing H_a .

Penetration of First Vortex

An important question for RF superconductivity is under what circumstances and at which applied magnetic field H_p the first vortex enters the superconductor, since the presence of even a few vortices can cause large losses. First

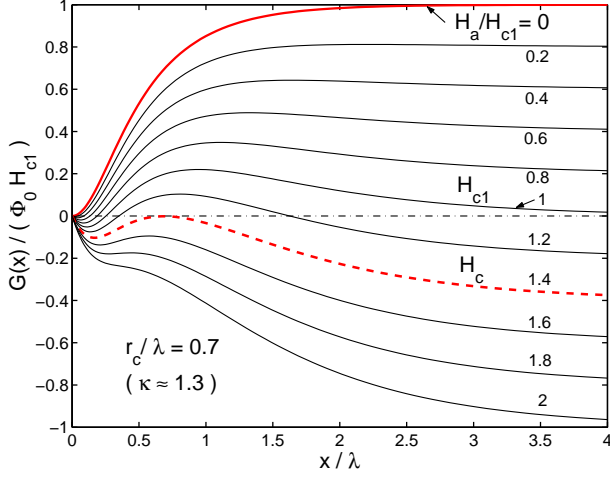


Figure 14: Gibbs free energy G of one vortex penetrating into a superconducting half space to a depth x , Eq. (22). Parameter is the applied field H_a in units of H_{c1} . The Bean-Livingston Barrier exists for $H_a < H_c$.

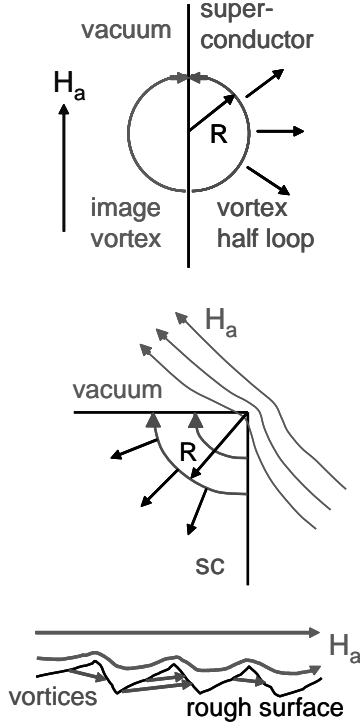


Figure 15: Nucleation of vortices as an arc of a circle at a planar surface (top), at a rectangular corner (middle), and at a rough surface (bottom, schematic).

I summarize the expressions for the three critical fields which for type-II superconductors (with $\kappa \geq 1/\sqrt{2}$) obey $B_{c1} \leq B_c \leq B_{c2}$:

$$\begin{aligned} B_{c1} &\approx \frac{\Phi_0}{4\pi\lambda^2} (\ln \kappa + \alpha), \\ B_c &= \frac{\Phi_0}{\sqrt{8}\pi\lambda\xi} = \frac{\sqrt{2}\kappa}{\ln \kappa + \alpha} B_{c1}, \end{aligned} \quad (20)$$

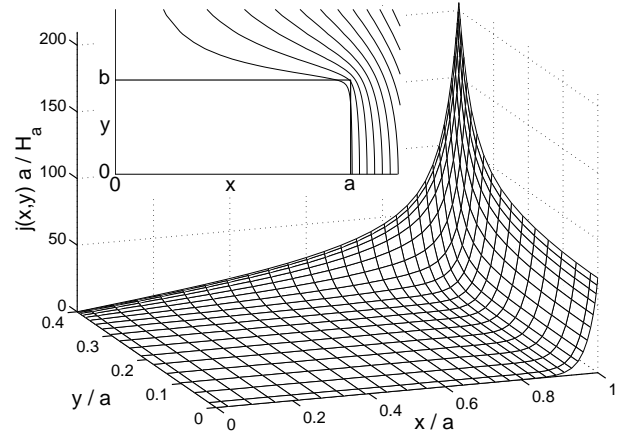


Figure 16: Supercurrents $j_z(x, y)$ in a bar with rectangular cross section $2a \times 2b$ ($b/a = 0.4$) in the Meissner state with London penetration depth $\lambda = 0.025a$. The currents (along the bar) are generated by a perpendicular applied uniform magnetic field $H_a \parallel z$ that penetrates to a depth λ . Shown is one quarter of the cross section. Note the high (but finite) peak of $j_z(x, y)$ at the corners. The inset shows the magnetic field lines.

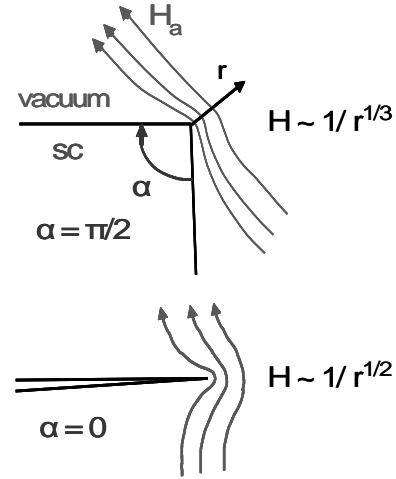


Figure 17: Field enhancement near the sharp edge of an ideal diamagnet.

$$\begin{aligned} B_{c2} &= \frac{\Phi_0}{2\pi\xi^2} = \sqrt{2}\kappa B_c, \\ \alpha(\kappa) &= \frac{1}{2} + \frac{1 + \ln 2}{2\kappa - \sqrt{2} + 2} = \begin{cases} 1.35, & \kappa = 0.71 \\ 0.50, & \kappa \gg 1. \end{cases} \end{aligned}$$

While the thermodynamic (B_c) and upper (B_{c2}) critical fields are exact, the lower critical field $B_{c1} = \mu_0 H_{c1}$ has to be calculated numerically from the self energy of a vortex of length L , $U_{\text{self}} = \Phi_0 H_{c1} L$. The function $\alpha(\kappa)$ is a good analytical fit to the numerical result of [10]. At $H_a = H_{c1}$ the nucleation of a vortex and motion to a depth $x \gg \lambda$ does not cost energy, see Fig. 14. However, the penetrating vortex has to surmount a barrier such that the field of first penetration H_p is larger than H_{c1} . This barrier was

Magnetic field H at the equator of:

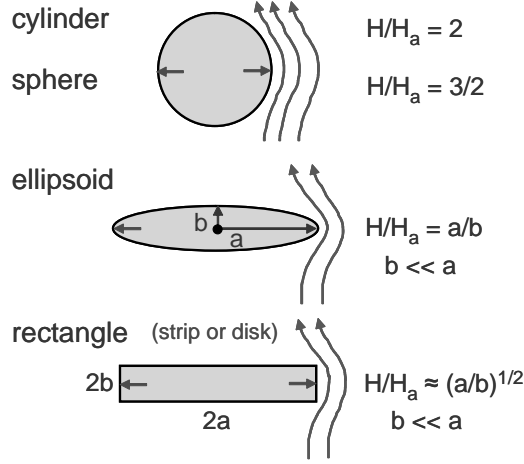


Figure 18: Enhancement of the magnetic field H at the equator of ideal diamagnetic cylinders, spheres, and strips of elliptic or rectangular cross section put in a uniform axial applied magnetic field H_a .

first predicted by Bean and Livingston (BL) [27] for a superconductor with planar surface in a parallel applied field H_a . The Gibbs free energy $G(x)$ for this case reads

$$G(x) = \Phi_0 \left(H_a e^{-x/\lambda} - \frac{1}{2} H_v(2x) + (H_{c1} - H_a) \right). \quad (21)$$

In it the first term is the interaction of the vortex with the applied field H_a or with its screening currents $(H_a/\lambda)e^{-x/\lambda}$, the second term is the interaction with the image vortex (at position $-x$, of opposite orientation), and the third term is an integration constant. Using the fact that for not too small κ one has $B_v(0) \approx 2B_{c1}$ (see Fig. 1) one has with Eq. (14), $B_{c1} \approx (\Phi_0/4\pi\lambda^2)K_0(r_c/\lambda)$ yielding with B_{c1} (20) a core radius $r_c \approx \xi \exp[-\alpha(\kappa)]$. With this we may write $G(x)$ (21) in the dimensionless form

$$\frac{G(x)}{\Phi_0 H_{c1}} \approx \frac{H_a}{H_{c1}} (e^{-x/\lambda} - 1) + 1 - \frac{K_0(\sqrt{4x^2 + r_c^2}/\lambda)}{K_0(r_c/\lambda)} \quad (22)$$

that is plotted in Fig. 14 for $\kappa \approx 1.3$. Of course, this $G(x)$ is a only approximate, in particular at small κ , for which vortex penetration has to be computed numerically. Anyway, Fig. 14 shows that vortex penetration becomes favorable at $H_a = H_c$ and that the Bean-Livingston barrier vanishes at $H_a \approx H_c > H_{c1}$.

The assumption of BL that the entering vortex is long, straight, and exactly parallel to a planar surface is not very realistic. Alternatively, one may assume that the first vortex nucleates and penetrates in form of a small loop, say a half circle of radius R , see Fig. 15 top. The self-energy of this half circle is approximately $U_{\text{self}} = \pi R (\Phi_0^2/4\pi\lambda^2\mu_0)$, putting the outer cut-off radius $\approx R$ instead of $\Lambda \gg R$ in the logarithm $\ln(\lambda/\xi) \rightarrow \ln(R/\xi) \approx 1$ when R is of order of ξ . The interaction of this vortex loop with the surface screening current of density j_s is $U_{js} \approx (\pi R^2/2)\Phi_0 j_s$

(flux quantum times loop area times j_s). For a planar surface one has $j_s = H_a/\lambda$ directly at the surface. The criterion that $U_{js} \geq U_{\text{self}}$ at $H_a \geq H_p$ yields then

$$H_p \approx \frac{\Phi_0/\mu_0}{2\pi\lambda R} = \frac{\sqrt{2}\xi}{R} H_c \approx H_c, \quad (23)$$

which is just the BL result. Thus, the assumption of a penetrating vortex loop does not change much the penetration field of a planar surface.

However, when the surface has roughness with characteristic length $\geq \xi$, then vortices will penetrate at sharp points or cusps, see Fig. 15. At a corner with angle $\alpha = 90^\circ$, the screening current directly at the surface is strongly enhanced at this corner; Fig. 16 shows this for a superconducting bar with square cross section $2a \times 2a$ and penetration depth $\lambda = 0.025a$, to which a uniform transverse H_a is applied. A rough estimate gives for this geometry an enhancement of the screening current at this corner, $j_s = CH_a/\lambda$, by a factor $C \approx 4$. The field of first vortex penetration H_p is then reduced from Eq. (23) by just this factor, $H_p \approx H_c/C \approx H_c/4$.

For sharper corners the enhancement of j_s and reduction of H_p are even larger. As shown in the textbook of Landau-Lifshitz (Electrodynamics of Continua) for an ideal diamagnetic material at a corner with angle α (Fig. 17) the magnetic field diverges as $H \propto 1/r^\beta$ with exponent $\beta = (\pi - \alpha)/(2\pi - \alpha)$, where r is the distance to the point of the corner. This gives $H \propto 1/r^{1/3}$ for $\alpha = \pi/2$ and $H \propto 1/r^{1/2}$ for $\alpha \rightarrow 0$.

Similarly, an axially applied magnetic field flowing around an ideal diamagnetic cylinder, sphere, or disks with elliptical or rectangular cross section of aspect ratio $b/a \ll 1$, is enhanced at its equator by factors 2, 3/2, a/b , or $\approx (a/b)^{1/2}$, respectively, due to the strong curvature of the field lines at this line, see Fig. 18.

Vortices in thin films

One has to distinguish two quite different types of vortices in thin film superconductors: vortices perpendicular or parallel to the film plane. In wide thin films with width $w = 2a \gg$ thickness $d = 2b$, the vortices will nearly always run perpendicular across the film thickness, even in tilted applied field H_a , because of the large demagnetization factor of this film. This means the circulating currents prefer to flow in the film plane. Only when H_a is exactly parallel to the film surface, or when the film is coating a bulk superconductor that screens any perpendicular field component, then vortices parallel to the film plane may occur.

When the film is of finite size, one may use Eqs. (19) to estimate at which applied perpendicular field component H_{az} the first vortices penetrate, namely already at a very small field, smaller than $H_{c1}\sqrt{d/w}$. When the film edges are wedge-shaped or sharp, the penetration field is even smaller, cf. Fig. 17 and Fig. 18 (elliptical edge). Into infinitely extended or closed films (e.g., a Nb layer covering the inner surface of a Cu cavity) any perpendicular field

will penetrate since the field lines cannot flow around the film. Only when this film has holes or slits can some magnetic flux cross the film via these holes, but the magnetic field in the holes will be larger than H_{az} by at least the ratio of film area over the total area of all holes. However, the field in the holes will penetrate into the film when it is of the order of H_{c1} times the square root of film thickness over hole distance. Thus, even such a perforated pin-free film will be penetrated by a perpendicular field that is very much smaller than H_{c1} . The peaked magnetic field, circulating current, and pair interaction of perpendicular vortices in thin films were calculated for infinitely extended [28] and finite-size (e.g. rectangular) films [26, 29, 30].

Pinning of vortices will not appreciably enhance all these penetration fields at high radio frequencies, where the (elastic) pinning forces are smaller than the viscous drag force. If the small applied perpendicular magnetic field is a DC field (e.g., some stray field or the earth magnetic field) then the additional RF field will even favor the penetration of the DC field in form of vortices, since it “shakes” the vortices. As shown in [31, 32], shaking of vortices by an AC field oriented perpendicular to the vortices leads to the relaxation of irreversible currents if the AC amplitude exceeds some threshold value. This vortex creep means that even in very small H_{az} , perpendicular vortices will penetrate under the action of a large-amplitude RF field, and then these vortices oscillate and dissipate energy.

The problem of parallel vortex lines in a thin film with $d \ll \lambda$ was solved by Alexei Abrikosov (1964), Vadim Shmidt (1969), and in an elegant way by Alex Gurevich [33]. The lower critical field is enhanced in thin films as compared to bulk superconductors,

$$B_{c1} = \frac{2\Phi_0}{\pi d^2} \left(\ln \frac{d}{\lambda} - 0.07 \right), \quad (24)$$

and the field at which the surface barrier for vortex penetration disappears is also enhanced,

$$B_p = \frac{\Phi_0}{2\pi d \xi}. \quad (25)$$

For example, a NbN film with $\xi = 5$ nm, $d = 20$ nm has $B_{c1} = 4.2$ T and $B_p = 6.37$ T, much better than the penetration field $B_p \approx B_c = 0.18$ T for Nb at low T .

To enhance the operating RF amplitude in microwave cavities for accelerators and reduce the losses, Gurevich [34] suggests to use solid Nb or Pb with multilayer coating on its inner surface by alternating superconducting and insulating layers with $d < \lambda$. This will prevent penetration of vortices into the bulk superconductor when the vortex penetration field B_p is large; e.g., for NbN films with $d = 20$ nm the RF field can be as high as 4.2 T. From the elastic and viscous forces on a parallel vortex in a thin film, Gurevich estimates its characteristic relaxation time as

$$\tau \approx 2d\mu_0\lambda^2/(\xi\rho_n). \quad (26)$$

For a 30 nm Nb₃Sn film this $\tau \approx 10^{-12}$ s is much shorter than the RF period of 10^{-9} s. The maximum amplitude

of the RF field at which the surface barrier of a single thin film coating disappears is of the order of the bulk H_c of the film material, e.g., 0.54 T for Nb₃Sn. Thus, Nb₃Sn coating more than doubles the vortex penetration field for Nb, $B_p \approx B_c = 0.18$ T at low T . It appears that Nb cavities coated with a Nb₃Sn layer or with NbN multilayers allow for much higher RF amplitudes than uncoated Nb, or Cu coated by a Nb film, if this can be achieved technically.

REFERENCES

- [1] M. Tinkham, “Introduction to Superconductivity”, Dover, New York 1996, p. 37 ff.
- [2] J. Bardeen, L. N. Cooper and J. Schrieffer, Phys. Rev. B 108 (1957) 1175.
- [3] D. C. Mattis and J. Bardeen, Phys. Rev. 111 (1958) 412.
- [4] A. A. Abrikosov, L. P. Gorkov and I. M. Khalatnikov, Sov. Phys. JETP 8 (1959) 182.
- [5] I. O. Kulik, in: Proc. of the 8th Workshop on RF Superconductivity, October 1997, Abano Terme (Padua), V. Palmieri and A. Lombardi eds, p. 283.
- [6] R. Brinkmann, M. Dohlus, D. Trines, A. Novokhatski, M. Timm, T. Weiland, P. Hülsmann, C. T. Riek, K. Scharnberg and P. Schmüser, “Terahertz Wakefields in the Superconducting Cavities of the TESLA-FEL Linac”, TESLA-Collaboration at DESY, Hamburg, Report 2000-07, March 2000.
- [7] J. R. Clem, J. Low Temp. Phys. 18 (1975) 427.
- [8] A. Yaouanc, P. Dalmas de Réotier and E. H. Brandt, Phys. Rev. B 55 (1997) 11107.
- [9] U. Essmann and H. Träuble, Phys. Lett. 24A (1967) 526; Sci. Am. 224 (1971) 75.
- [10] E. H. Brandt, Phys. Rev. Lett. 78 (1997) 2208; E. H. Brandt, Phys. Rev. B 68 (2003) 054506.
- [11] G. Carneiro and E. H. Brandt, Phys. Rev. B 61 (2000) 6370.
- [12] E. H. Brandt, Phys. Rev. B 71 (2005) 014521.
- [13] J. Bardeen and M. J. Stephen, Phys. Rev. A 140 (1965) 2634.
- [14] M. Tinkham, Phys. Rev. Lett. 13 (1964) 804.
- [15] A. Schmid, Phys. Kondensierten Materie 5 (1966) 302.
- [16] C. R. Hu and R. S. Thompson, Phys. Rev. B 6 (1972) 110.
- [17] A. I. Larkin and Yu. N. Ovchinnikov, in: “Nonequilibrium Superconductivity”, D. N. Langenberg and A. I. Larkin, eds (Elsevier, Amsterdam 1986) p. 493.
- [18] A. M. Campbell and J. E. Evetts, Adv. Phys. 21 (1972) 199.
- [19] E. H. Brandt, Rep. Prog. Phys. 58 (1995) 1465-1594.
- [20] G. Blatter, M. V. Feigelmann, M. V. Geschkenbein, A. I. Larkin, and V. M. Vinokur, Rev. Mod. Phys. 66 (1994) 1125-1388.
- [21] J. I. Gittleman and B. Rosenblum, Phys. Rev. Lett. 16 (1968) 734.
- [22] E. Zeldov et al., Phys. Rev. Lett. 73 (1994) 1428.
- [23] E. H. Brandt, Phys. Rev. B 59 (1999) 3396; Phys. Rev. B 60 (1999) 11939; Physica C 332 (2000) 99.

- [24] E. H. Brandt, Phys. Rev. B 58 (1998) 6506; 6523.
- [25] E. H. Brandt, Phys. Rev. B 64 (2001) 024505.
- [26] E. H. Brandt, Phys. Rev. B 72 (2005) 024529.
- [27] C. P. Bean and J. D. Livingston, Phys. Rev. Lett. 12 (1964) 14.
- [28] J. Pearl, Appl. Phys. Lett. 5 (1964) 65.
- [29] E. H. Brandt, Phys. Rev. B 79 (2009) 134526.
- [30] E. Sardella and E. H. Brandt, Supercond. Sci. Technol. 23 (2010) 025015.
- [31] G. P. Mikitik and E. H. Brandt, Phys. Rev. B 69 (2004) 134521; Phys. Rev. B 67 (2003) 104511.
- [32] E. H. Brandt and G. P. Mikitik, Phys. Rev. Lett. 89 (2002); Superconductor Sci. Technol. 17 (2004) 1.
- [33] G. Stejic, A. Gurevich, E. Kadyrov, D. Christen, R. Joynt, and D. C. Larbalestier, Phys. Rev. B 49 (1994) 1247.
- [34] A. Gurevich, Appl. Phys. Lett. 88 (2006) 012511.